Design of Infrared Laser Pulses for the Vibrational De-excitation of Translationally Cold Li$_2$ Molecules[†]

Qinghua Ren

Department of Pure and Applied Chemistry, University of Strathclyde, 295 Cathedral Street, Glasgow, G1 1XL, U.K.

Gabriel G. Balint-Kurti*

School of Chemistry, University of Bristol, Bristol BS8 1TS, U.K.

In connection with attempts to form molecular Bose−Einstein condensates, there have been reports in the literature of the preparation of samples of translationally cold alkali metal dimers. The molecules in these samples are generally in excited vibrational levels. To form a stable Bose−Einstein condensate, the molecules must be de-excited to their lowest vibrational state. In this paper, we demonstrate that through the use of optimal control theory, it is possible to design a sequence of infrared laser pulses that will de-excite a sample of ^{7}Li$_2$ molecules from the $v = 10$ vibrational level of their $^1\Sigma_g^+$ ground electronic state to their lowest $v = 0$ vibrational level with an overall efficiency of 91.1%.

I. Introduction

The first Bose−Einstein condensates of trapped ultracold atoms were reported in 1995,[1−3] and their formation and properties continue to be an active area for research.[4,5] More recently, attempts to form Bose−Einstein condensates of molecular species have attracted great interest from both an experimental and theoretical perspective.[6−14] In this context, the greatest efforts have been directed at the formation of translationally cold samples of alkali metal dimers.[14−19] In all cases, however, the translationally cold samples of alkali dimer molecules are formed either in their highest vibrational level[9,20−22] or in quite highly excited vibrational levels.[15,16]

To form a stable, molecular Bose−Einstein condensate, it will be essential for the molecules in the sample to be in their lowest vibrational levels; otherwise, the energy present as vibrational excitation will be transformed through molecular collisions into relative translational motion and will result in loss from the sample. Both Stwalley[23] and Koch et al.[24] have suggested mechanisms for achieving the required de-excitation by using a Raman process involving excitation to an intermediate excited electronic state. In the case of Koch et al.,[24] they also performed optimal control calculations to design a laser pulse that could efficiently achieve the desired de-excitation. Experimentally, Viteau et al.[25] have successfully demonstrated the cooling of a sample of translationally cold Cs$_2$ molecules using a shaped broadband excitation to promote the molecule to an excited electronic state and then to permit it to spontaneously decay. The shaping of the excitation frequency spectrum ensures the depletion of population from excited vibrational levels and the consequent build-up of population in the lowest vibrational level with each excitation-spontaneous decay cycle.

In 2001, Tolra et al.[16] showed that it is possible to form a sample of translationally cold Cs$_2$ molecules in a well-defined vibrational−rotational level, lying well below the ground state dissociation limit, by using a stimulated Raman photoassociation

process on a sample of cold Cs atoms in a magneto-optical trap. In a previous publication, we have shown that it is possible to design a sequence of infrared laser pulses to efficiently de-excite H$_2$ molecules from their highest to their lowest vibrational level.[26] In the present publication, we extend this work and demonstrate that it is possible to design a sequence of infrared laser pulses to de-excite the alkali dimer ^{7}Li$_2$ from a high-lying vibrational level ($v = 10$) to its ground vibrational level.

Our approach is based on the application of the electric−nuclear Born−Oppenheimer (ENBO) approximation[27,28] which enables us to take account of the molecule−laser field interaction to all orders in the field strength. The laser pulses are designed using optimal control theory,[29,30] as described in detail in previous publications.[26−28] The time-dependent quantum dynamics, used as part of the optimal control calculations, are treated in a fully three-dimensional manner. The numerical techniques used to solve the time-dependent Schrödinger equation are based on the use of a grid representation of the time-evolving wavepackets in coordinate space and in the conjugate momentum space.

The plan of the paper is as follows: the details of the theoretical methods used are described in Section II; the results of the numerical calculations are presented in Section III, and a short conclusion is given in Section IV.

II. Theory

In this section, a brief description is given of the ab initio molecular electronic structure methods used for the calculation of the electronic energy of the Li$_2$ molecule and its interaction with the electric field of the laser. The methods used for the time-dependent quantum dynamics in three dimensions and the optimal control theory are also briefly reviewed.

A. Ab Initio Molecular Electronic Structure Calculations. The ab initio calculations of the molecular potential energy under the influence of an electric field are performed using the MOLPRO computer code.[31] In keeping with the theory of the ENBO approach,[27] the electronic energy of the ^{7}Li$_2$ molecule

---

is computed as a function of the strength of an external electric field, the orientation of the diatomic with respect to the field, and the internuclear separation.

The electric field is taken to point in the positive z direction, which coincides with the polarization direction of the field, and the $^7Li_2$ molecule is oriented at different angles with respect to this direction. The field strength was allowed to range from 0 to 0.0040 atomic units (a.u.) (0−0.2056 V $Å^{-1}$) in increments of 0.0005 a.u. The internuclear separation ranged from 1.6 to 33.0 bohr in steps of 0.2 bohr. The angle of the $^7Li_2$ molecular axis with the field direction is varied over the range 0−90° in intervals of 10°. The ab initio calculations were performed using a CASSCF[32] (two active valence orbitals) followed by a MRCI(SD)[33] calculation with a cc-pVQZ atomic orbital basis set.[34] No Davidson correction[35] was applied to the MRCI energies.

B. Solution of the Time-Dependent Schrödinger Equation. The Fourier grid Hamiltonian method[36,37] is used to compute the radial part of the wave functions of the initial state and the target state. The nuclear wave function is represented on a two-dimensional grid in the radial internuclear coordinate, R, and in the polar angle, θ, which the molecular axis makes with the field polarization direction. The R grid points are chosen to be evenly spaced, and the θ grid points are the Gauss-Legendre quadrature points.[38,39] In the present study, because we take the field direction to specify the z axis and because there are no azimuthal forces present capable of changing the azimuthal, ϕ, dependence of the nuclear wave function, we can effectively ignore this variable. The time-dependent Schrödinger equation is solved using the split operator method.[40,41] The action of the radial part of the kinetic energy operator on the wave function is computed using the fast Fourier transform method advocated by Kosloff,[42,43] whereas the action of the polar-angle-dependent part of the kinetic energy operator is computed using the discrete variable representation of Light et al.[44]

The nuclear dynamics of the Li_2 molecule under the influence of the time-varying electric field is treated by solving the time-dependent Schrödinger equation:

$$i\frac{\partial \psi(\mathbf{R}, t)}{\partial t} = \{\hat{T}_{nu}(\mathbf{R}) + V(\mathbf{R}, \varepsilon(t))\}\,\psi(\mathbf{R}, t) \qquad (1)$$

where

$$\hat{T}_{nu}(\mathbf{R}) = -\frac{1}{2\mu_{Li_2}}\nabla_R^2 \qquad (2)$$

Here $V(\mathbf{R}, \varepsilon)$ is the eigenvalue of the electronic Schrödinger equation for a fixed value of the nuclear coordinates, R; the electric field, ε; and the angle, θ; between the field and the axis of the diatomic; $\mathbf{R} \equiv (R, \theta, \phi)$ is the relative position vector of one Li nucleus with respect to the other and the angles θ, ϕ describe the orientation of the Li_2 molecular axis with respect to the z axis (i.e., the field direction). Further discussion of eq 1 and its solution can be found in refs 27 and 28.

To take account of the possibility of molecular dissociation induced by exciting the vibrational motion of the diatomic into the continuum during the propagation process, we include a negative imaginary absorbing potential[45] operating in the last 2 bohr of the range of the internuclear separation; that is, for the $^7 Li_2$ molecule from 31 to 33 bohr.

We used a quadratic absorbing potential, which is of the general form[45]

$$V(\bar{R}) = -iA_2\left[\frac{3}{2}\bar{R}^2\right] \qquad (3)$$

where $\bar{R} = R/L$, ($0 \le R \le L$), and L is the "damping" length of the grid (here, it is equal to 2.0 bohr). The strength parameter is $A_2 = 2.750E$, where E is the relative kinetic energy of the dissociating molecule. Here, we take this to be the energy spacing between the highest two vibrational energy levels below the dissociation limit (5.78 cm^{-1} for Li_2).

C. Optimal Control Theory. Our aim is to design a laser pulse that drives a system from an initial state, $\psi(t = 0)$, to a final target state, Φ, at a fixed time $t = T$. The laser field is optimized so as to transform the wave function as completely as possible from the specified initial state to the specified final state. We follow the optimal control theory as set out by Rabitz and co-workers.[29] We define an objective function, J, of the form

$$J(\varepsilon) = \left|\langle\psi(T)|\Phi\rangle\right|^2 - \alpha_0\int_0^T [\varepsilon(t)]^4\,dt -$$
$$2Re\left\{\int_0^T\left\langle\chi(t)\left|\frac{\partial}{\partial t} + i\hat{H}(R, \varepsilon(t))\right|\psi(t)\right\rangle dt\right\} \qquad (4)$$

where $\psi(t)$ is the wave function of the system; Φ is the wave function of the target state; $\chi(t)$ is an undetermined Lagrange multiplier which assures that the system satisfies the time-dependent Schrödinger equation; and $\hat{H}(R, \varepsilon(t))$ is Hamiltonian, including the matter radiation interaction. The second term on the right-hand side of the equation is a penalty function for the fluence, or integrated laser field strength. We set the weight of this penalty term, α_0, to 150 in the present case.

The electric field, $\varepsilon(t)$, is defined as having two parts: an immutable envelope function, $s(t)$, and a part, $\varepsilon_0(t)$, which will be varied to achieve the desired control objective; that is,

$$\varepsilon(t) = s(t)\,\varepsilon_0(t) \qquad (5)$$

With these definitions, we maximize the objective functional, $J(\varepsilon)$, using a conjugate gradient method.

It is important to restrict the maximum field amplitude to keep it below the value where significant ionization might occur. To prevent the algorithm from sampling the $\varepsilon_0(t)$ values outside of the range [ε_{min}, ε_{max}] during the line search, the magnitude of the incremental change, $d^k(t)$, to the field magnitude at the kth iteration is projected as follows:[46,28]

$$d_p^k(t) = P(\varepsilon^k(t) + d^k(t)) - \varepsilon^k(t) \qquad (6)$$

Here, the projector, $P(x)$, is defined as

$$\begin{aligned} P(x) &= sign(x)\,x_{lim} &&\text{if}\quad |x| > x_{lim} \\ P(x) &= x &&\text{if}\quad x \in [-x_{lim}, x_{lim}] \end{aligned} \qquad (7)$$

where x_{lim} is some number less than ε_{max} and the dynamic range of the electric field is assumed to be symmetric about zero; that is, $\varepsilon_{min} = -\varepsilon_{max}$.

To restrict the frequency content of the optimized field to a predefined range,[47] the projected search direction $d_p^k(t)$ is first transformed from a time- to a frequency-dependent quantity using the fast Fourier transform method,[42,43] and then the
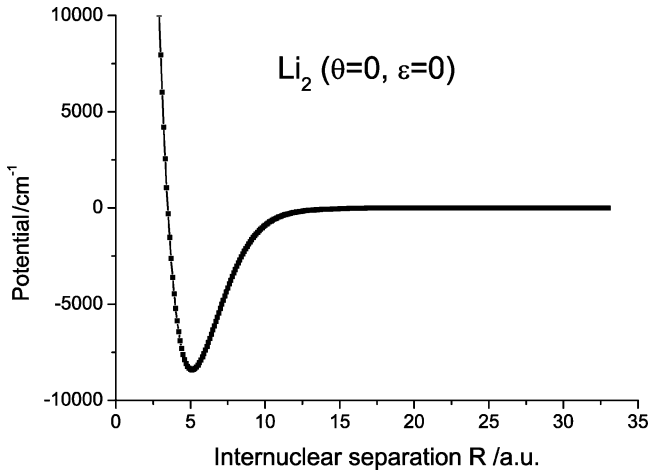
Figure 1. Ab initio calculated potential of the $^1\Sigma_g^+$ ground electronic state of Li$_2$ at orientational angle $\theta = 0°$ and electric field $\varepsilon = 0$.

frequency spectrum is filtered using a 20th-order Butterworth bandpass filter;[48] that is,

$$h(\omega) = \left\{ \left[1 + \left(\frac{\omega_1}{\omega} \right)^{40} \right] \left[1 + \left(\frac{\omega}{\omega_h} \right)^{40} \right] \right\}^{-1/2} \quad (8)$$

where ω_1 and ω_h are the low and high cutoff frequencies and are set at $\omega_1 = 0.5 \times 10^{11}$ s^{-1} and $\omega_h = 5.0 \times 10^{13}$ s^{-1}, respectively.

The resulting frequency spectrum is then transformed back to the projected electric field using the reverse fast Fourier transform method.

The conjugate gradient iterations for the optimization of the objective function, J (see eq 4), are deemed to have converged when the absolute value of the ratio of J evaluated at successive iterations, that is, $|J_k/J_{k+1}|$, has converged to within a value of 10^{-6}.

III. Results

Because we consider highly excited vibrational states in the present work, the internuclear separation of the two atoms might reach relatively larger values, extending even into the asymptotic region where the potential becomes flat. The ab initio calculated potential energy for the $^1\Sigma_g^+$ ground electronic state of Li$_2$ in the absence of the electric field is shown in Figure 1. We consider internuclear separations of the Li$_2$ molecule ranging from 1.6 to 33.0 bohr. The calculated binding energy, D_0, of the Li$_2$ molecule is 1.022 eV (8239.7 cm^{-1}), as compared to an experimentally measured value[49] of 1.04 eV. Using the Fourier grid Hamiltonian (FGH) method,[36] we get 41 bound vibrational states for the Li$_2$ molecule from its ground vibrational state Li$_2$($v = 0$) to the highest calculated bound vibrational state Li$_2$($v = 40$). The highest vibrational energy level for Li$_2$($v = 40$) lies 1.39 cm^{-1} below the dissociation limit. The calculated energies of the lowest 11 vibrational levels are given in Table 1. The calculated separation of the lowest two levels is 341.60 cm^{-1}, as compared with an experimental value[49] of ω_e of 351.43 cm^{-1}. Our estimate of the equilibrium separation from our calculated data points is 5.1 Bohr, as compared with the experimentally reported[49] value of 5.0511 Bohr. Table 2 lists the grid parameters and other details needed for the solution of the time-dependent Schrödinger equation.

Table 3 summarizes the results of the action of the optimized laser pulses, obtained using the optimal control formalism

TABLE 1: Lowest 11 Calculated Vibrational Energy Levels of Li$_2$

vibrational quantum number	energy/cm^{-1}
0	0
1	341.595 699 2
2	678.071 636 3
3	1009.387 143
4	1335.495 522
5	1656.344 218
6	1971.873 198
7	2282.016 232
8	2586.698 242
9	2885.835 635
10	3179.335 754

TABLE 2: Details of Grid and Other Parameters Used in the Solution of the Time-Dependent Schrödinger Equation

parameter	
range of molecular bond length (bohr)	1.6−33.0
number of radial grid points	256
number of angular grid points	8
total time/ps	23.22
number of time steps	524288

TABLE 3: Results of the Optimal Control Calculations for Li$_2$ Rovibrational De-excitation from ($v = 10, j = 0$) to ($v' = 0, j' = 0$), Step by Step[a]

$i \rightarrow f$	initial field strength, ε_0/a.u.	initial frequency, $\omega_0/10^{13}$ Hz	optimal yield/%	max ε/a.u.	no. of iterations
10 → 9	0.0010	0.8799	99.17	0.000 867	47
9 → 8	0.0008	0.8799	99.05	0.001 019	36
8 → 7	0.0008	0.9298	99.04	0.001 111	57
7 → 6	0.0010	0.9298	99.23	0.000 956	21
6 → 5	0.0008	0.9619	98.87	0.000 991	43
5 → 4	0.0012	0.9776	98.59	0.001 967	56
4 → 3	0.0010	0.9776	99.07	0.000 919	25
3 → 2	0.0012	1.0087	99.04	0.001 371	16
2 → 1	0.0015	1.0087	99.06	0.001 470	17
1 → 0	0.0010	1.0241	99.64	0.001 047	14
10 → 0			91.13	0.001 967	

[a] The optimization parameters are given in the text.

described above, for the de-excitation processes from the high-lying vibrational state ($v = 10, j = 0$) down to the ground vibrational state ($v = 0, j = 0$), step by step. All these results are obtained corresponding to a pulse length of 23.22 ps divided into $N_t = 524\ 288$ time steps.

In the following subsections, we present and discuss the computed optimized laser pulses in more detail.

A. Li$_2$($v = 10, j = 0$) → Li$_2$($v' = 0, j' = 0$) De-excitation, Step by Step. The initial trial laser field for the $v_{i+1} \rightarrow v_i$ de-excitation process is set as

$$\varepsilon(t) = \varepsilon_0 \cos(\omega_0 t/2)\, s(t) \quad (9)$$

where ω_0 was generally set at $(E_{i+1} - E_i)/h$, corresponding to the calculated $v_{i \rightarrow i+1}$ transition frequency in Li$_2$. It was subsequently found, however, that the use of initial frequency values corresponding to a neighboring transition sometimes gave slightly improved results. The values of the initial frequency, ω_0, actually used are quoted in Table 3. The initial electric field amplitude, ε_0, is also shown in the table. The envelope function is
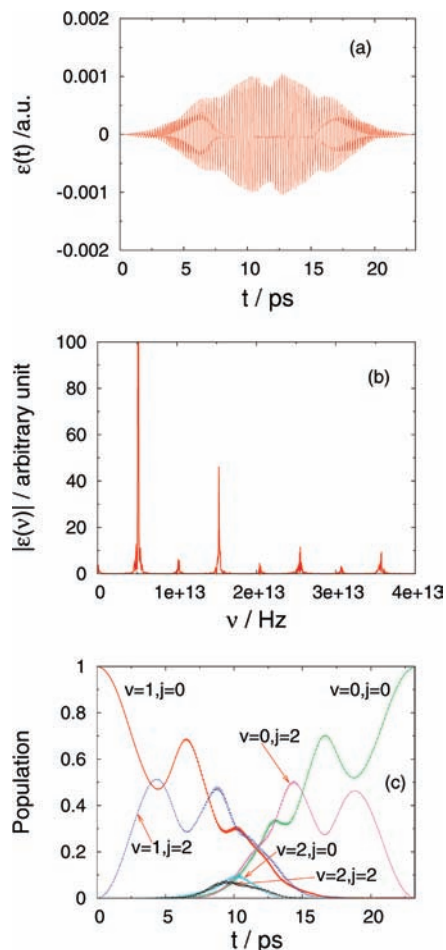
$$s(t) = \sin^2(\pi t/T) \quad (10)$$

Figure 2. (a) The optimized electric field as a function of time for the $Li_2(v = 1, j = 0) \rightarrow Li_2(v' = 0, j' = 0)$ de-excitation. (b) The spectrum for the optimized electric field. (c) The change in populations of the initial, target, and other states shown as a function of time.

Figure 3. (a) The optimized electric field as a function of time for the $Li_2(v = 10, j = 0) \rightarrow Li_2(v' = 9, j' = 0)$ de-excitation. (b) The spectrum for the optimized electric field. (c) The change in populations of the initial, target, and other states shown as a function of time. Other two small unlabeled populations correspond to the $(v = 11, j = 0)$ and $(v = 11, j = 2)$ states.

where the pulse duration is $T = 23.22$ ps. $x_{lim} \equiv \varepsilon_{max}$ in eq 6 was generally set equal to $2.0 \times \varepsilon_0$.

Table 3 shows the optimal yields (transition probabilities) for the vibrational de-excitation from the high-lying vibrational state $Li_2(v = 10, j = 0)$ down to the ground vibrational state $Li_2(v = 0, j = 0)$, step by step. It can be seen that the transition probabilities for all of the 10 de-excitation processes are close to or even greater than 99%. The maximum electric field strength in atomic units (a.u.), which arises in the optimized time-varying electric field and which does not exceed 0.001967 au (0.1011 V Å^{-1}), is also shown in the table. The high transition probabilities achieved through the use of optimal control theory suggest that the system is fully controllable. In this case, it would, in principle, be possible to attain 100% transformation efficiency for each of the optimized laser pulses,[50] provided all the constraints (e.g., on the electric field amplitude and frequency range) were lifted.

According to the data shown in Table 3, the optimized laser pulse can yield a total probability of 91.13% for the de-excitation of the Li_2 molecule from its high-lying $(v = 10, j = 0)$ vibrational−rotational state to its ground $(v = 0, j = 0)$ state, and the maximum value of the electric field in the sequence of optimized pulse required is only 0.001 967 au (0.1011 V Å^{-1}).

Figure 2a shows the converged optimized electric field as a function of time for the de-excitation process from the rovibrational state $(v = 1, j = 0)$ down to the rovibrational state $(v' = 0, j' = 0)$, and the absolute value of its Fourier transform
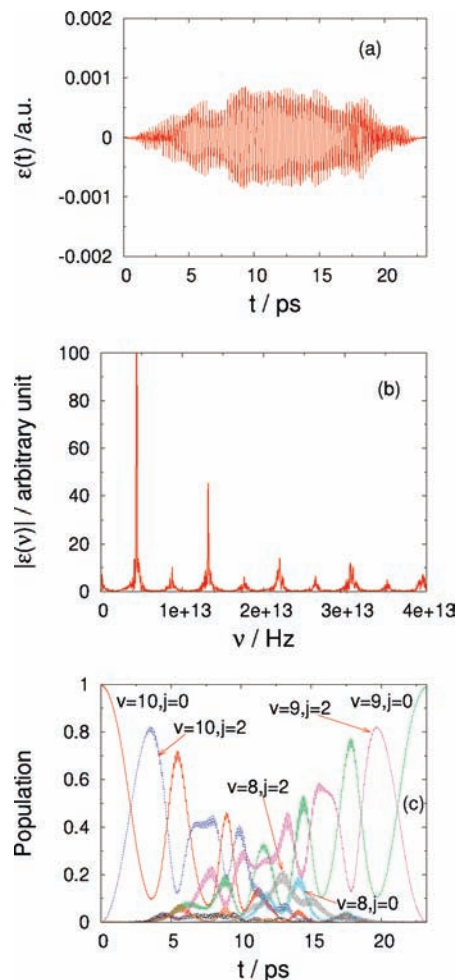
is shown in Figure 2b. It can be seen that the main contribution to the frequency spectrum is centered around the frequency $\nu = \nu_{0,1}/2 = 0.5120 \times 10^{13}$ s^{-1}, which corresponds to half of the $\nu_{0\rightarrow1}$ transition energy and is the same as the initial guessed value. This confirms our initial assumption that the major mechanism for the de-excitation process is via a two-photon stimulated emission. The optimization process has introduced a second significant contribution at a frequency of $\nu = 3\nu_{0,1}/2 = 1.5361 \times 10^{13}$ s^{-1}. This suggests that a secondary mechanism for the de-excitation takes place via a two-photon Raman process with a virtual excitation at a frequency of $\nu_{0,1}/2$ and a de-excitation at a frequency of $3\nu_{0,1}/2$. Figure 2c shows the populations of the initial $(v = 1, j = 0)$ rovibrational state, the target rovibrational state $(v' = 0, j' = 0)$, and several other states as a function of time over the duration of the laser pulse. The figure shows that the de-excitation process proceeds through an initial rotational excitation to the $(v' = 1, j' = 2)$ state. Population in the $(v' = 0, j' = 0)$ target state starts to build up only half way through the pulse, and this happens simultaneously with the build-up also in the population in other states, particularly the $(v' = 0, j' = 2)$ state. Eventually, the population is all steered into the $(v' = 0, j' = 0)$ target state by the end of the pulse.

Figure 3a shows the converged optimized electric field as a function of time for the de-excitation process from the rovi-

TABLE 4: Results of the Optimal Control Calculations for Li$_2$ Rovibrational De-excitation from ($v = i$, $j = 0$) to ($v' = f$, $j' = 0$)[a]

$i \rightarrow f$	initial field strength, ε_0/a.u.	initial frequency, ω_0/10^{13} Hz	optimal yield /%	max ε/a.u.	no. of iterations
10 → 7	0.0010	0.9134	95.69	0.001269	29
7 → 5	0.0008	0.9459	96.68	0.001012	48
5 → 3	0.0010	0.9619	97.03	0.001092	14
3 → 0	0.0015	0.9933	96.19	0.001841	19
10 → 0			86.35	0.001841	

[a] The optimization parameters are given in the text.

brational state ($v = 10$, $j = 0$) to ($v' = 9$, $j' = 0$). The Fourier transform method is used to generate the spectrum of the laser pulse, which is shown in Figure 3b. It can be seen that the frequency spectrum is mainly centered around the frequency $\nu = \nu_{9\rightarrow10}/2 = 0.4399 \times 10^{13}$ s^{-1}, which corresponds to the half of $\nu_{9\rightarrow10}$ transition energy and is the same as the initially guessed value. The optimization process has introduced a second major contribution at a frequency of $\nu = 3\nu_{9,10}/2 = 1.3198 \times 10^{13}$ s^{-1}. This suggests, in analogy with the discussion above, that a contributory mechanism for the de-excitation might involve a two-photon Raman process in which there is an initial excitation to an excited virtual state lying at an energy corresponding to a frequency of $\nu = \nu_{9,10}/2$ above the ($v = 10$, $j = 0$) level followed by a de-excitation to the target level. Figure 3c shows the populations of the different states during the laser pulse. As population leaves the ($v = 10$, $j = 0$) level, it is first transferred to the ($v' = 10$, $j' = 2$) state. The populations in the ($v' = 9$, $j' = 2$) and ($v' = 9$, $j' = 0$) levels build up at a slightly later time. At intermediate times, several other states, including ($v' = 8$, $j' = 0$), ($v' = 8$, $j' = 2$), ($v' = 11$, $j' = 0$) and ($v' = 11$, $j' = 2$), are populated to a small extent. At the end of the pulse, the population ends up nearly entirely in the ($v' = 9$, $j' = 0$) target level.

The other eight de-excitation processes from the rovibrational state ($v = 9$, $j = 0$) down to the rovibrational state ($v = 1$, $j = 0$) shown in Table 3 are generally similar to the above, so they are not discussed in detail.

We have also checked de-excitation from some higher vibrational levels and have been able to design laser pulses to efficiently achieve these processes, as well (i.e., ($v = 11$, $j = 0$) → ($v = 10$, $j = 0$) 99.18%, ($v = 12$, $j = 0$) → ($v = 11$, $j = 0$) 99.31%).

B. Li$_2$ ($v = 10$, $j = 0$) → Li$_2$($v' = 0$, $j' = 0$) De-excitation Using Fewer Laser Pulses. In ref 26, a useful and interesting observation which we made during the investigation of the hydrogen de-excitation process was that an initial guess of the form of eq 9 generally converged successfully to give an optimized laser pulse that would efficiently excite a $\Delta v = 1$ transition or de-excite a $\Delta v = -1$ transition. We also found that it was often possible to start with such an initially guessed pulse and to use the optimal control procedures to obtain an optimized laser pulse that de-excited the system by more than a single vibrational quantum. This conclusion also holds true in the case of Li$_2$.

After checking many different possible de-excitation processes, we have been able to find a reasonably efficient sequence of four laser pulses that is able to de-excite Li$_2$($v = 10$, $j = 0$) to its lowest level. Table 4 shows the optimal yields for the sequence of vibrational de-excitation processes to de-excite Li$_2$ starting with the high-lying vibrational state ($v = 10$, $j = 0$) and ending with the ground vibrational state ($v = 0$, $j = 0$), which gives a good overall de-excitation probability. The bottom
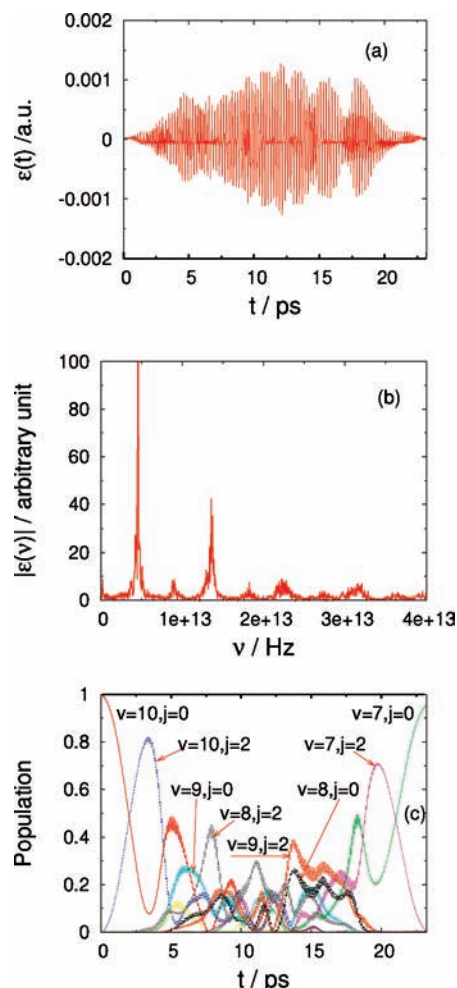

Figure 4. (a) The optimized electric field as a function of time for the Li$_2$($v = 10$, $j = 0$) → Li$_2$($v' = 7$, $j' = 0$) de-excitation. (b) The spectrum for the optimized electric field. (c) The change in populations of the various states as a function of time. In the center of the laser pulse, some population also goes to the ($v = 11$, $j = 0$), ($v = 11$, $j = 2$), ($v = 6$, $j = 0$), and ($v = 6$, $j = 2$) states, which are not shown.

line of the table shows the overall yield for the entire sequence of 4 pulses required for the de-excitation process ($v = 10$, $j = 0$) → ($v = 0$, $j = 0$).

From the data in Table 4, it can be seen that it is possible to design a sequence of four laser pulses, each of 23.22 ps duration, which will de-excite the Li$_2$ molecule from its high-lying rovibrational state ($v = 10$, $j = 0$) to its ground state ($v = 0$, $j = 0$) with an overall probability of 86.35%. The maximum electric field strength does not exceed 0.001 841 au (0.0946 V Å^{-1}).

Our proposed de-excitation mechanism consists of a sequence of four pulses with no phase relationship to each other. The main frequency component of each pulse increases monotonically (i.e, proceeding down the third column from the left of Table 4), and the overall process may be viewed as a type of linearly chirped pulse.

Figure 4a shows the converged optimized electric field as a function of time for the de-excitation process from the rovibrational state ($v = 10$, $j = 0$) to the ($v = 7$, $j = 0$) state, and the absolute value of its Fourier transform is shown in Figure 4b. The frequency spectrum is centered mainly at the frequency $\nu = \nu_{7\rightarrow8}/2 = 0.4567 \times 10^{13}$ s^{-1}, which corresponds to the half of $\nu_{7\rightarrow8}$ transition energy, and is the same as the initial guessed value. The optimization process has introduced a second major

contribution at a frequency of $\nu = 3\nu_{7,8}/2 = 1.3701 \times 10^{13}$ s^{-1}. Figure 4c shows the populations of the various states as a function of time over the duration of the laser pulse. Populations also go to the states $(v = 10, j = 2)$, $(v = 9, j = 2)$, $(v = 9, j = 0)$, $(v = 8, j = 2)$, $(v = 8, j = 0)$, and $(v = 7, j = 2)$ in the center of the laser pulse, but these nearly completely disappear before the end of the laser pulse. Furthermore, some small population is also present in the states $(v = 11, j = 0)$, $(v = 11, j = 2)$, $(v = 6, j = 0)$, and $(v = 6, j = 2)$ in the center of the laser pulse, but these are not labeled explicitly.

The other three de-excitation processes shown in Table 4 are similar and are not discussed in detail.

IV. Conclusions

We have explored the possibility of using a sequence of shaped infrared laser pulses to de-excite a sample of $^7\text{Li}_2$ molecules from a relatively high lying rotational−vibrational state, $(v = 10, j = 0)$, to its ground rotational−vibrational state without any intermediate excitation to another electronic state.

We have designed a sequence of 10 laser pulses, each of 23.22 ps duration, which can de-excite a sample of Li$_2(v = 10, j = 0)$ to Li$_2$ $(v = 0, j = 0)$ with an overall probability of 91.13% or a sequence of four laser pulses that can accomplish the same process with an overall probability of 86.35%. The main frequency component of each pulse increases monotonically as the de-excitation proceeds, and the overall process may be viewed as a type of linearly chirped composite pulse. The high transition probabilities achieved through the use of optimal control theory suggest that the system is fully controllable.

Our results show that such a sequence of infrared laser pulses might be effectively used as a method of removing residual vibrational energy from a sample of translationally cold alkali dimer molecules in relatively high lying vibrational states and might therefore be used to play a role in the ultimate formation of a molecular Bose−Einstein condensate.

References and Notes

(1) Anderson, M. H.; Ensher, J. R.; Matthews, M. R.; Wieman, C. E.; Cornell, E. A. *Science* **1995**, *269* (5221), 198.

(2) Davis, K. B.; Mewes, M. O.; Andrews, M. R.; van Druten, N. J.; Durfee, D. S.; Kurn, D. M.; Ketterle, W. *Phys. Rev. Lett.* **1995**, *75*, 3969.

(3) Bradley, C. C.; Sackett, C. A.; Tollett, J. J.; Hulet, R. G. *Phys. Rev. Lett.* **1995**, *75*, 1687.

(4) Robert, A.; Sirjean, O.; Browaeys, A.; Poupard, J.; Nowak, S.; Boiron, D.; Westbrook, C. I.; Aspect, A. *Science* **2001**, *292* (5516), 461.

(5) Anglin, J. R.; Ketterle, W. *Nature* **2002**, *416*, 211.

(6) Doyle, J. M.; Friedrich, B. *Nature* **1999**, *401*, 749.

(7) Wynar, R.; Freeland, R.; Han, D.; Ryu, C.; Heinzen, D. *Science* **2000**, *287*, 1016.

(8) Williams, C. J.; Julienne, P. S. *Science* **2000**, *287*, 986.

(9) Donley, E. A.; Claussen, N. R.; Thompson, S. T.; Wieman, C. E. *Nature* **2002**, *417*, 529.

(10) Herbig, J.; Kraemer, T.; Mark, M.; Weber, T.; Chin, C.; Nägerl, H. C.; Grimm, R. *Science* **2003**, *301*, 1510.

(11) Vanhaecke, N.; de Souza Melo, W.; Tolra, B. L.; Comparat, D.; Pillet, P. *Phys. Rev. Lett.* **2002**, *89*, 063001.

(12) Cvitas, M. T.; Soldan, P.; Hutson, J. M.; Honvault, P.; Launay, J.-M. *J. Phys. Chem.* **2007**, *127*, 074302.

(13) Pichler, M.; Stwalley, W. C.; Beuc, R.; Pichler, G. *Phys. Rev. A* **2004**, *69*, 013403.

(14) Dulieu, O.; Raoult, M.; Tiemann, E. *J. Phys. B* **2006**, *39*, 19.

(15) Fioretti, A.; Comparat, D.; Crubellier, A.; Dulieu, O.; Masnou-Seeuws, F.; Pillet, P. *Phys. Rev. Lett.* **1998**, *80*, 4402.

(16) Tolra, B. L.; Drag, C.; Pillet, P. *Phys. Rev. A* **2001**, *64*, 061401.

(17) Dion, C. M.; Drag, C.; Dulieu, O.; Tolra, B. L.; Masnou-Seeuws, F.; Pillet, P. *Phys. Rev. Lett.* **2001**, *86*, 2253.

(18) Gabbanini, C.; Fioretti, A.; Lucchesini, A.; Gozzini, S.; Mazzoni, M. *Phys. Rev. Lett.* **2000**, *84*, 2814.

(19) Xu, K.; Mukaiyama, T.; Abo-Shaeer, J. R.; Chin, J. K.; Miller, D. E.; Ketterle, W. *Phys. Rev. Lett.* **2003**, *91*, 210402.

(20) Julienne, P. S.; Tiesinga, E.; Kohler, T. *J. Mod. Opt.* **2004**, *51*, 1787.

(21) McKenzie, C.; Denschlag, J. H.; Häffner, H.; Browaeys, A.; de Araujo, L. E. E.; Fatemi, F. K.; Jones, K. M.; Simsarian, J. E.; Cho, D.; Simoni, A.; Tiesinga, E.; Julienne, P. S.; Helmerson, K.; Lett, P. D.; Rolston, S. L.; Phillips, W. D. *Phys. Rev. Lett.* **2002**, *88*, 120403.

(22) Cubizolles, J.; Bourdel, T.; Kokkelmans, S. J. J. M. F.; Shlyapnikov, G. V.; Salomon, C. *Phys. Rev. Lett.* **2003**, *91*, 240401.

(23) Stwalley, W. *Eur. Phys. J. D* **2004**, *31*, 221.

(24) Koch, C. P.; Palao, J. P.; Kosloff, R.; Masnou-Seeuws, F. *Phys. Rev. A* **2004**, *70*, 013402.

(25) Viteau, M.; Chotia, A.; Allegrini, M.; Bouloufa, N.; Dulieu, O.; Comparat, D.; Pillet, P. *Science* **2008**, *321*, 232.

(26) Ren, Q.; Balint-Kurti, G. G.; Manby, F.; Artamonov, M.; Ho, T.; Rabitz, H. *J. Chem. Phys.* **2006**, *125*, 021104.

(27) Balint-Kurti, G. G.; Manby, F.; Ren, Q.; Artamonov, M.; Ho, T.; Rabitz, H. *J. Chem. Phys.* **2005**, *122*, 084110.

(28) Ren, Q.; Balint-Kurti, G. G.; Manby, F.; Artamonov, M.; Ho, T.; Rabitz, H. *J. Chem. Phys.* **2006**, *124*, 014111.

(29) Shi, S.; Rabitz, H. *J. Chem. Phys.* **1990**, *92*, 364.

(30) Balint-Kurti, G. G.; Zou, S.; Brown, A. *Adv. Chem. Phys.* **2008**, *138*, 43.

(31) *MOLPRO, version 2002. 1*, a package of ab initio programs. Werner, H.-J.; Knowles, P. J.; Lindh, R.; Schütz, M.; Celani, P.; Korona, T.; Manby, F. R.; Rauhut, G.; Amos, R. D.; Bernhardsson, A.; Berning, A.; Cooper, D. L.; Deegan, M. J. O.; Dobbyn, A. J.; Eckert, F.; Hampel, C.; Hetzer, G.; Lloyd, A. W.; McNicholas, S. J.; Meyer, W.; Mura, M. E.; Nicklass, A.; Palmieri, P.; Pitzer, R.; Schumann, U.; Stoll, H.; Stone, A. J.; Tarroni, R.; Thorsteinsson, T. 2002.

(32) Werner, H.-J.; Knowles, P. J. *J. Chem. Phys.* **1985**, *82*, 5053.

(33) Werner, H.-J.; Knowles, P. J. *J. Chem. Phys.* **1988**, *89*, 5803.

(34) Dunning, T. H., Jr. *J. Chem. Phys.* **1989**, *90*, 1007.

(35) Langhoff, S. R.; Davidson, E. R. *Int. J. Quantum Chem.* **1974**, *8*, 61.

(36) Marston, C. C.; Balint-Kurti, G. G. *J. Chem. Phys.* **1989**, *91*, 3571.

(37) Balint-Kurti, G. G.; Ward, C. L.; Marston, C. C. *Comput. Phys. Commun.* **1991**, *67*, 285.

(38) Press, W. H.; Flannery, B. P.; Teukolsky, S. A.; Vetterling, W. T. In *Numerical Recipes*; Cambridge U. P.: Cambridge, MA, 1986.

(39) Offer, A. R.; Balint-Kurti, G. G. *J. Chem. Phys.* **1994**, *101*, 10416.

(40) Feit, M. D.; Fleck, J. A., Jr. *J. Chem. Phys.* **1983**, *78*, 301.

(41) Feit, M. D.; Fleck, J. A., Jr. *J. Chem. Phys.* **1984**, *80*, 2578.

(42) Kosloff, D.; Kosloff, R. *J. Comp. Phys.* **1983**, *52*, 35.

(43) Kosloff, R. *J. Phys. Chem.* **1988**, *92*, 2087.

(44) Light, J. C.; Hamilton, I. P.; Lill, V. J. *J. Chem. Phys.* **1985**, *82*, 1400.

(45) Vibok., A.; Balint-Kurti, G. G. *J. Phys. Chem.* **1992**, *96*, 8712.

(46) Birgin, E. G.; Martínez, J. M.; Raydan, M. *SIAM J. Optim.* **2000**, *10*, 1196.

(47) Gross, P.; Neuhauser, D.; Rabitz, H. *J. Chem. Phys.* **1992**, *96*, 2834.

(48) Rabiner, L. R., Rader, C. M., Eds. *Digital Signal Processing*; IEEE Press selected reprint series; IREEE press: New York, 1972.

(49) Huber, K. P.; Herzberg, G. *Molecular Spectra and Molecular Structure IV. Constants of Diatomic Molecules*; Van Nostrand Reinhold Co.: New York, 1979.

(50) Rabitz, H. A.; Hsieh, M. M.; Rosenthal, C. M. *Science* **2004**, *303*, 1998.